Int. J. Heat Mass Transfer. Vol. 25, No. 10, pp. 1489–1502, 1982
Printed in Great Britain

0017-9310/82/101489-14 $03.00/0

INTERACTION BETWEEN A STREAM WHICH PASSES THROUGH AN ENCLOSURE AND NATURAL CONVECTION WITHIN THE ENCLOSURE

E. M. SPARROW and F. SAMIE
Department of Mechanical Engineering, University of Minnesota, Minneapolis, MN 55455, U.S.A.

(*Received* 13 *November* 1981 *and in final form* 11 *February* 1982)

Abstract—An analysis has been made of the fluid flow and heat transfer in a vertically oriented cylindrical enclosure in whose lower and upper walls there are small apertures through which fluid passes into and out of the enclosure. The throughflow stream induces a recirculating flow in the enclosure. Furthermore, natural convection motions are induced in the enclosure owing to the temperature difference between the entering stream and the enclosure walls. The strengths of the forced and natural convection flows are respectively characterized by the Reynolds and Rayleigh numbers, and the latter may be either positive or negative depending on whether or not the wall temperature T_w exceeds the entering fluid temperature T_0. When the throughflow stream is vertically upward, positive-Rayleigh-number natural convection (i.e. $T_w > T_0$) opposes the throughflow-driven recirculation and reduces the heat transfer in the range of small and intermediate Rayleigh numbers. At high Rayleigh numbers, the throughflow stream is overpowered by the natural convection, with resulting high values of heat transfer. For negative Rayleigh numbers (i.e. $T_w < T_0$), the heat transfer is little different from that for zero Rayleigh number.

NOMENCLATURE

D, diameter of cylindrical enclosure;
d, diameter of inlet and exit apertures;
g, acceleration of gravity;
H, height of enclosure;
k, thermal conductivity;
P, dimensionless pressure, equation (3);
Pr, Prandtl number;
p, pressure;
p', reduced pressure, $(p + \rho_0 gz)$;
Q, surface-integrated heat transfer rate;
q, local heat flux;
R, dimensionless radial coordinate, r/D;
Ra, Rayleigh number, equation (5);
Re, Reynolds number of inflow, equation (11);
r, radial coordinate;
T, temperature;
T_0, temperature of entering fluid;
T_w, temperature of enclosure walls;
U, V, dimensionless velocity components, equation (3);
U_i, dimensionless inlet velocity, $\bar{V}_z D/\nu$;
V_r, radial velocity component;
V_z, axial velocity component;
$\bar{V}_z$, inflow velocity;
Z, dimensionless axial coordinate, z/D;
z, axial coordinate.

Greek symbols

β, thermal expansion coefficient;
θ, dimensionless temperature, $(T - T_0)/(T_w - T_0)$;
ν, kinematic viscosity;
ρ, density;
ρ_0, density of entering flow;
ψ, stream function.

INTRODUCTION

THIS paper is concerned with the interaction between a fluid stream which passes through an enclosed space and natural convection motions which may occur in the space, with the natural convection being induced by temperature differences between the stream and the walls of the enclosure. Problems of this general type are widely encountered in the real world. For example in the oven of an electric stove there is a throughflow of air which usually enters the oven cavity via a slot at the bottom edge of the oven door and exits via an aperture embedded in one of the burners on the surface of the stove. The air entering the oven cavity is at room temperature while the walls of the cavity are typically at a temperature that is elevated by several hundred degrees. This temperature difference will induce natural convection motions which, depending on the velocity magnitudes involved, may influence the path of the throughflow stream and the temperature distribution in the cavity. A second illustration is the interaction between the natural convection recirculation in an attic and the throughflow which enters via soffit vents and exits via roof vents. Other examples which occur in industrial processes may also be cited.

The aforementioned examples are intended to illustrate the class of problems on which attention is to be focused, but they are characterized by highly specific geometrical configurations and are therefore inappropriate for a general research-type study. A more

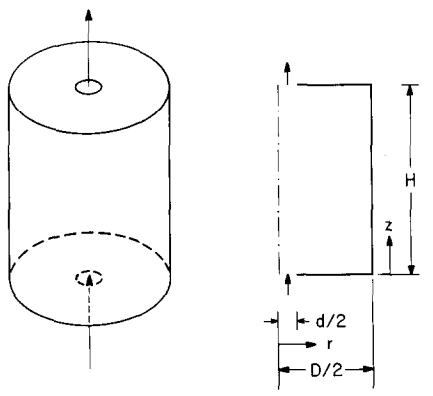

FIG. 1. Vertically oriented circular cylinder with fluid throughflow.

generic problem has been selected to explore the nature of the interactions between the throughflow and natural convection recirculation.

The problem chosen for study is illustrated at the left in Fig. 1. The basic geometry is a hollow, vertically oriented circular cylinder, with small circular apertures centered in its upper and lower faces. For concreteness, the figure portrays a fluid stream which enters the cylindrical enclosure via the lower aperture and exits via the upper aperture, but the reversed flow direction is also covered by the analysis and results. The entering fluid has a temperature T_0, while the inner walls of the cylinder are at a different uniform temperature T_w. The two cases $T_w > T_0$ and $T_w < T_0$ are dealt with in this paper.

The problem is governed by several dimensionless parameters. Two of these are related to the fluid flow—the Reynolds number Re of the throughflow and the Rayleigh number Ra of the natural convection in the enclosure. There are two geometrical parameters, d/D and H/D, respectively the ratio of the aperture diameter to the cylinder diameter and the ratio of the cylinder height to diameter. The fifth parameter is the Prandtl number.

For the analysis it is sufficient to fix the direction of the throughflow as shown in the figure and to regard the Reynolds number as positive for that direction. The Rayleigh number can be either positive or negative, depending on the sign of $(T_w - T_0)$. If the throughflow were to be reversed in direction relative to that of Fig. 1, the results can be obtained from those presented here by reversing the sign of $(T_w - T_0)$. Thus, for example, the results for an upward throughflow with $T_w > T_0$ are identical to those for a downward throughflow with $T_w < T_0$.

Even when natural convection effects are negligible (i.e. small Ra), the anticipated pattern of fluid flow within the enclosure is quite complex. In particular, the throughflow stream gives rise to a large scale recirculatory motion which washes the walls of the enclosure. At higher Rayleigh numbers, the natural convection flow within the enclosure interacts with the aforementioned recirculation and, at still higher Rayleigh numbers, it may interact with the throughflow stream itself. Thus, for a given Reynolds number of the throughflow, it is of interest to identify the Rayleigh numbers at which these interactions occur.

Furthermore, it is relevant to determine the effect of the fluid flow interactions on the wall heat transfer. A first impression might suggest that since the condition $T_w > T_0$ corresponds to a natural convection upflow along the vertical (cylindrical) wall, natural convection would enhance the heat transfer for an upward-directed throughflow, with $T_w < T_0$ having the opposite effect. Such a view, however, neglects the fact that the large-scale recirculation that is driven by the throughflow actually moves downward along the vertical wall. Thus, from physical reasoning alone, there is some uncertainty about whether $T_w > T_0$ or $T_w < T_0$ (i.e. positive or negative Rayleigh number) gives rise to heat transfer enhancement.

Quantitative fluid flow and heat transfer results for the problem were obtained from numerical solutions performed with an elliptic finite-difference program (an elliptic program was mandatory because of the recirculating flow). Laminar flow conditions were assumed to prevail. For the solutions, attention was focused on the effects of the Reynolds and Rayleigh numbers for a fixed geometrical configuration. For a given value of the Reynolds number, the Rayleigh number was varied from -10^6 to 10^6. The Prandtl number was assigned a value of 0.7, which corresponds to air.

Results for the fluid flow and temperature fields will be presented in terms of streamline and isotherm maps. Distributions of the local heat flux along the walls of the enclosure are presented graphically, while the surface-integrated heat transfer rates are tabulated.

ANALYSIS

Governing equations and parameters

The problem will be formulated in r, z cylindrical coordinates under the assumption of axisymmetry. The buoyancy force which drives the natural convection motion will be derived by rearrangement of the body force and pressure gradient terms which appear in the z-momentum equation, namely, $(-\partial p/\partial z - \rho g)$. If the terms $\rho_0 g$ and $-\rho_0 g$ are added to the contents of the foregoing parentheses and if $p' = p + \rho_0 g z$, there follows

$$-\partial p/\partial z - \rho g = -\partial p'/\partial z + g(\rho_0 - \rho). \quad (1)$$

If the Boussinesq equation of state, $(\rho_0 - \rho) = \beta\rho(T - T_0)$, is employed, equation (1) becomes

$$-\partial p/\partial z - \rho g = -\partial p'/\partial z + g\beta\rho(T - T_0). \quad (2)$$

In equation (2), the buoyancy force $g\beta\rho(T - T_0)$ is readily identified, while $\partial p'/\partial z$ is the gradient of a reduced pressure.

Equation (2) is then substituted into the z-momentum equation, whereafter the assumption of negligible fluid property variations is invoked for all the governing equations, which include the continuity

equation, the r and z momentum equations, and the energy equation. These equations are then made dimensionless via the definitions

$$U = V_z D/\nu, \quad V = V_r D/\nu, \quad P = p'(\rho\nu^2/D^2), \quad (3)$$

$$\theta = (T - T_0)/(T_w - T_0), \quad R = r/D, \quad Z = z/D, \quad (4)$$

$$Ra = (g\beta(T_w - T_0)D^3/\nu^2)Pr, \quad Pr = c_p\mu/k. \quad (5)$$

The dimensionless conservation equations then emerge as

$$\partial(RV)/\partial R + \partial(RU)/\partial Z = 0, \quad (6)$$

$$U(\partial V/\partial Z) + V(\partial V/\partial R) = -\partial P/\partial R + \nabla^2 V - (V/R^2), \quad (7)$$

$$U(\partial U/\partial Z) + V(\partial U/\partial R) = -\partial P/\partial Z + \theta(Ra/Pr) + \nabla^2 U, \quad (8)$$

$$U(\partial\theta/\partial Z) + V(\partial\theta/\partial R) = (1/Pr)\nabla^2\theta \quad (9)$$

where ∇^2 is the R, Z Laplace operator. The essential character of these equations has not been changed by the transformation of variables—they remain partial differential equations. The two dimensionless parameters that have emerged are Ra and Pr.

The other parameters follow from the specification of the enclosure geometry and of the velocity of the throughflow stream. For the geometry specification, it is necessary to give the values of

$$d/D \quad \text{and} \quad H/D. \quad (10)$$

The inlet velocity of the throughflow will be assumed uniform and equal to $\bar{V}_z$. Correspondingly, the dimensionless inlet velocity U_i is $\bar{V}_z D/\nu$, which can be written as

$$U_i = (D/d)Re, \quad Re = \bar{V}_z d/\nu \quad (11)$$

where Re is the Reynolds number of the throughflow. By specifying Re and (d/D), the dimensionless inlet velocity U_i is fixed.

The statement of the governing equations and the dimensionless parameters is now complete. Attention will now be turned to the procedure used to solve the equations.

Solution methodology

As noted earlier, the recirculating nature of the flow causes the problem to be elliptic and therefore an elliptic finite-difference method was used for the solutions. The specific method was that of Patankar, which is described in a book-length exposition [1], so little elaboration is needed here. The method works with the so-called primitive variables (velocities, pressure, and temperature) rather than with derived variables such as the stream function and vorticity. A special feature of the method is that the grid points at which the velocity components are computed are displaced from those at which the pressure and temperature are computed. In such a staggered grid arrangement, the pressure difference between two adjacent grid points serves as the driving force for the velocity component located between these two grid points, which would not be true if the grids were not staggered. The staggering also leads to a more rational finite-difference form of the continuity equation.

The boundary conditions that were employed in conjunction with the finite-difference code will now be described. On all solid boundaries, the velocity components U and V are zero and the temperature $\theta = 1$, while on the centerline of the enclosure (a symmetry line), $V = \partial U/\partial R = \partial\theta/\partial R = 0$. The inflow boundary (i.e. the aperture through which the flow enters the enclosure) is characterized by the conditions $U = (D/d)Re$, $V = \theta = 0$.

It remains to specify the conditions at the outflow boundary (i.e. the aperture through which the flow exits the enclosure). Except for very simple problems, it is a general truism that the conditions at an outflow boundary are not known to a high degree of precision. Indeed, precise knowledge of the happenings at an outflow boundary can usually be obtained only by solving for the flow and temperature fields in the region downstream of the boundary, a task that is normally beyond the scope of the problem being considered. In view of this state of affairs, a common practice is to impose simple conditions at the outflow boundary and to structure the grid so that the impact of the selected conditions does not penetrate very far into the solution domain.

In the present problem, a heavy concentration of grid points was deployed in the neighborhood of the outflow boundary, with the immediately adjacent points being displaced from the boundary by a dimensionless distance of 0.0025 (the range of Z is from 0 to 1). The presence of this grid point concentration enabled the velocity and temperature fields to shuck off the influence of the outflow boundary conditions within a small distance from the boundary.

The outflow boundary conditions were as follows

$$V = \partial\theta/\partial Z = 0, \quad (12)$$

$$U(R, Z_0) = U(R, (Z_0 - \Delta Z)) + \text{constant} \quad (13)$$

where Z_0 is the Z coordinate of the outflow boundary and $(Z_0 - \Delta Z)$ is the Z coordinate of the boundary-adjacent grid points. The numerical value of the constant was found by satisfying global mass conservation.

A 31×31 grid was used for the numerical solutions, with the grid layout being tailored to the specifics of the velocity field. The tailoring was performed on the basis of preliminary computer runs. In the R direction, the points were more heavily concentrated across the throughflow stream and adjacent to the outer wall of the enclosure. In the Z direction, the heaviest concentration of points was positioned adjacent to the upper boundary (including the outflow boundary), with a lesser concentration adjacent to the lower boundary.

The attainment of convergence is a commonly encountered difficulty in natural convection enclosure

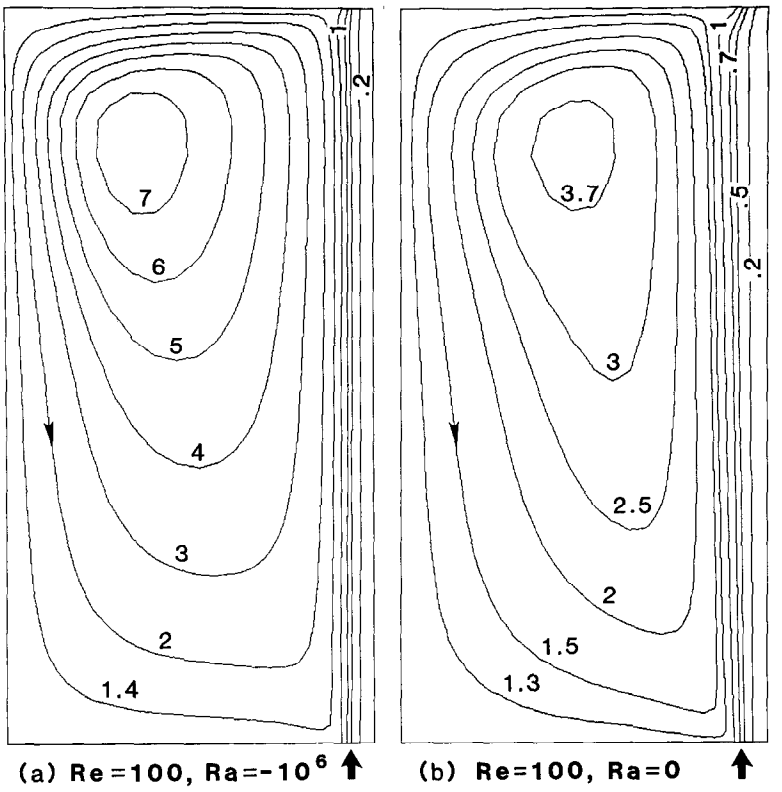

FIG. 2. Streamline maps for $Re = 100$, with $Ra = -10^6$ and 0. The curve parameter is $\psi/\nu D$.

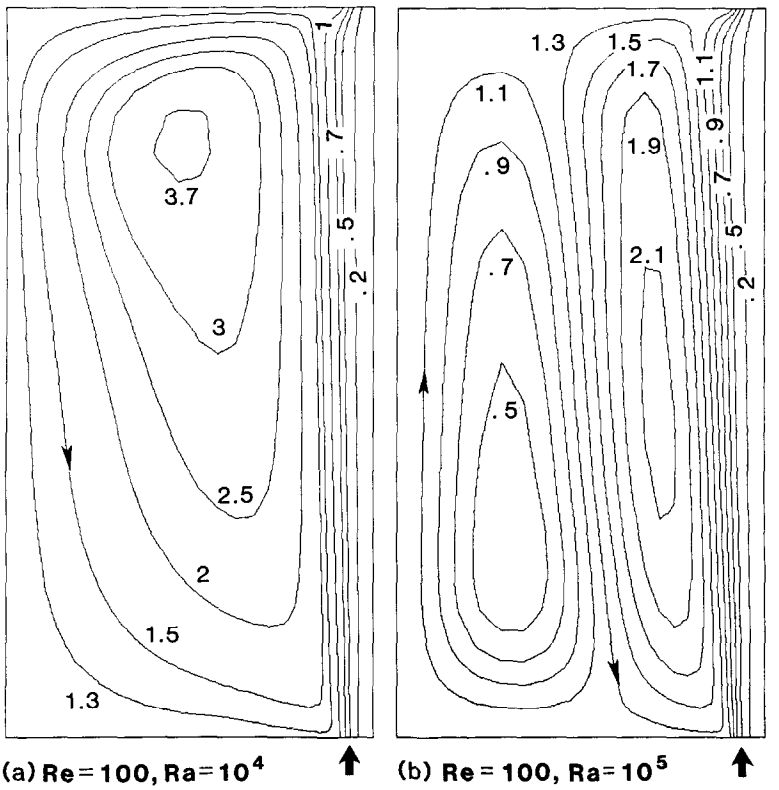

FIG. 3. Streamline maps for $Re = 100$, with $Ra = 10^4$ and 10^5. The curve parameter is $\psi/\nu D$.

problems. As an aid to convergence, the various Rayleigh number cases for a given Reynolds number were computed successively, starting with $Ra = 0$ and proceeding to higher values of $|Ra|$. The converged output for a given Rayleigh number was used as input for the next Rayleigh number.

Underrelaxation of U, V, and θ was employed to avoid divergence. For $|Ra| \leq 10^4$, the computations were started with an underrelaxation factor of 0.5, and this was increased in successive steps to a terminal value of 0.9 based on visual observation of the print-out of a convergence index. For the higher Rayleigh numbers, the initial relaxation factor was either 0.2 or 0.3, which was stepped up to a final value of 0.9.

Presentation parameters

The flow pattern within the enclosure will be displayed in streamline maps, while the temperature field will be presented in isotherm contour diagrams. In both instances, dimensionless variables are used, respectively

$$\psi/\nu D \text{ and } (T - T_0)/(T_w - T_0). \tag{14}$$

With regard to heat transfer, results will be presented for the distributions of the local heat flux on each wall of the enclosure, for the surface-integrated heat transfer rate at each wall, and for the overall heat transfer rate for all the walls. The dimensionless forms to be used in reporting these quantities are

$$qD/k(T_w - T_0) \text{ and } Q/kD(T_w - T_0). \tag{15}$$

RESULTS AND DISCUSSION

As noted in the Introduction, attention will be focused here on the effects of the fluid flow parameters Re and Ra for a fixed enclosure geometry. In selecting the geometry, it appeared most reasonable to work with a square-like enclosure, i.e. $H/D = 1$. Also, since the apertures that are encountered in practice are small compared with the surface area of the enclosure, the d/D ratio was chosen to be 0.1.

The assumption of laminar flow and the recognition that jet-like flows (the throughflow stream has a jet-like character) are relatively unstable suggests that parametrically assigned Reynolds numbers, in order to be realistic, should be small. Correspondingly, Reynolds numbers equal to 100 and 250 were employed in the calculations. For each Reynolds number, the Rayleigh number was varied systematically from -10^6 to 10^6, with 11 Ra values used for $Re = 100$ and 12 Ra values for $Re = 250$. For all cases, $Pr = 0.7$.

Patterns of fluid flow

Streamline maps showing the patterns of fluid flow in the enclosure are presented in Figs. 2–4 for $Re = 100$ and in Figs. 5 and 6 for $Re = 250$. Each figure conveys results for two Rayleigh numbers in a side-by-side presentation. These streamline maps, six for $Re = 100$ and four for $Re = 250$, taken from a larger available set, were judged to be the minimum number for documenting the evolving flow pattern.

In each graph, the throughflow stream is seen to enter at the lower right and exit at the upper right. The symmetry line of the enclosure forms the right-hand boundary of each graph. The respective graphs are arranged in the order of increasing Rayleigh number.

Initial consideration will be given to the results for $Re = 100$ and, as a point of departure, attention will be focused on the case of pure forced convection ($Ra = 0$) which is depicted in the right-hand graph of Fig. 2. As seen in the graph, the throughflow stream passes through the enclosure as a tight bundle, spreading only slightly as it moves upward. Just upstream of the exit aperture, the stream contracts in order to accommodate to the aperture diameter. The throughflow induces a large recirculating eddy in which the flow moves radially outward near the top of the enclosure, downward along the side (vertical) wall, and inward near the bottom wall. These directions are noteworthy, especially that along the vertical wall, because they can be compared with the expected directions of motion of a natural-convection-induced flow.

When $T_w < T_0$, the resulting buoyancy will induce a downflow along the vertical wall of the enclosure. Such a flow will reinforce the recirculating eddy that is driven by the throughflow. Therefore, for $Ra < 0$, which corresponds to $T_w < T_0$, the flow pattern for $Ra = 0$ should be preserved, but with higher recirculation velocities. An examination of the left-hand graph of Fig. 2, which corresponds to $Ra = -10^6$, affirms this expectation. The results for Rayleigh numbers between 0 and -10^6 lie between those shown in Fig. 2.

For the situation in which $T_w > T_0 (Ra > 0)$, the buoyancy tends to induce an upflow along the vertical wall, which opposes the throughflow-driven recirculation. However, there is a range of Rayleigh numbers where the buoyancy is too weak to materially affect the flow pattern. Thus, as seen in the left-hand diagram of Fig. 3, the flow pattern for $Ra = 10^4$ is virtually identical to that for $Ra = 0$ (note that the indicated streamline values are the same for the two cases).

At Rayleigh numbers higher than 10^4, the buoyancy progressively plays a stronger and stronger role. At $Ra = 10^5$, as seen in the right-hand graph of Fig. 3, it overpowers the throughflow-driven recirculation in the outer reaches of the enclosure, with the result that the flow adjacent to the outer wall is vertically upward. However, the buoyancy is still not able to dominate the entire flow field in the enclosure. Instead, there are co-existing side-by-side eddies, one driven by the buoyancy and the other driven by the throughflow.

At $Ra = 2 \times 10^5$ (left-hand diagram, Fig. 4), the buoyancy really begins to influence the results. It draws a portion of the throughflow stream to the outer wall via a circuitous path that skirts the fringes of the much-diminished inner eddy. When the thus-displaced portion of the throughflow stream arrives at the outer wall, it is propelled upward along the wall and then, near the top of the enclosure, it moves radially inward and exits via the aperture.

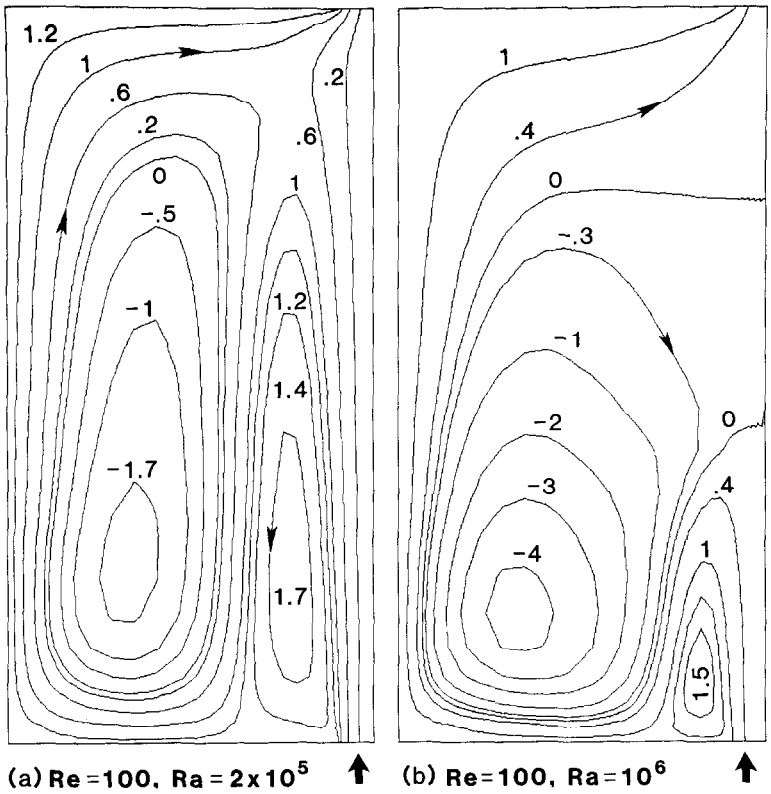

FIG. 4. Streamline maps for $Re = 100$, with $Ra = 2 \times 10^5$ and 10^6. The curve parameter is $\psi/\nu D$.

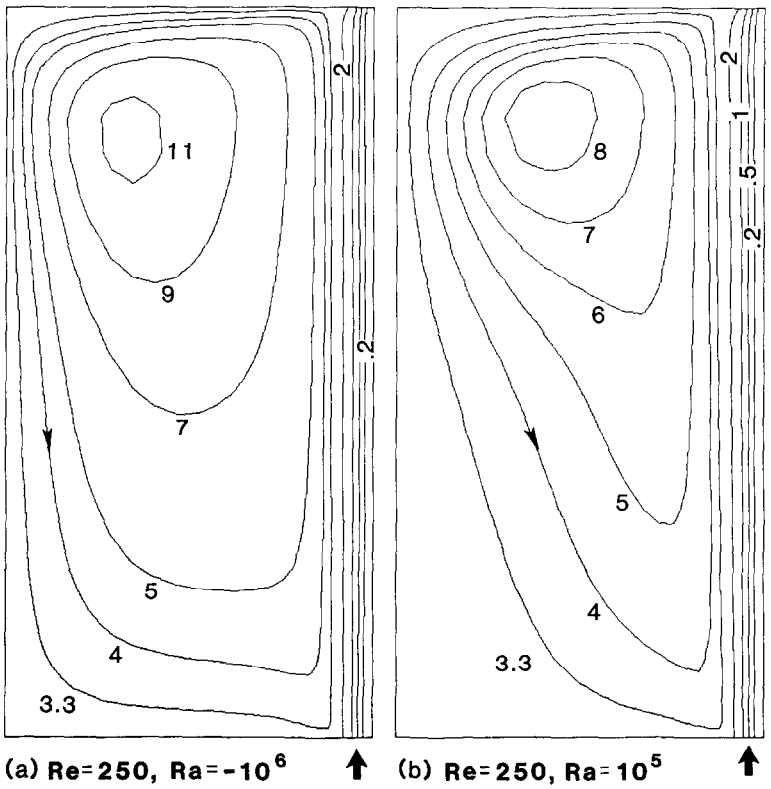

FIG. 5. Streamline maps for $Re = 250$, with $Ra = -10^6$ and 10^5. The curve parameter is $\psi/\nu D$.

The buoyancy attains full mastery of the flow in the enclosure at $Ra = 10^6$ (right-hand diagram, Fig. 4). As seen there, the entirety of the throughflow stream is drawn toward the outer wall and remains in the outer reaches of the enclosure during most of its passage.

The foregoing chronicle of the evolution of the flow in the enclosure suggests a number of heat transfer ramifications. Relative to the overall heat transfer for $Ra = 0$, it is expected that negative Rayleigh numbers would yield enhancement, while small and intermediate positive Rayleigh numbers should bring about a reduction in heat transfer. At large positive Rayleigh numbers, where the entire throughflow stream is drawn to the outer wall, significant enhancement may be expected. These conjectures will be revisited shortly when a tabulation of heat transfer results is presented.

Attention will now be turned to the flow patterns for $Re = 250$, which are portrayed in Figs. 5 and 6. In view of the higher value of the Reynolds number now being considered (250 compared to 100), it is to be expected that lesser buoyancy effects will be encountered over the investigated Rayleigh number range, -10^6 to 10^6. Thus, in Fig. 5, it is seen that the flow pattern is hardly affected by the Rayleigh number in the range from -10^6 to 10^5. At $Ra = 2 \times 10^5$ (Fig. 6, left-hand graph), the buoyancy is able to create a small eddy with a wall-adjacent upflow but, clearly, the throughflow-driven recirculation still holds sway. At $Ra = 10^6$ (right-hand graph), the buoyancy-induced eddy has grown significantly and is now the dominant recirculation in the enclosure. The throughflow stream, however, still remains intact, which is in sharp contrast to the annihilation of the stream in evidence in the right-hand diagram of Fig. 4.

Based on these flow patterns, it can be expected that the heat transfer results for $Re = 250$ will be much less affected by the Rayleigh number than will the results for $Re = 100$.

Temperature field

Representative temperature field information, expressed in terms of contours of the dimensionless temperature θ, is presented in Figs. 7 and 8 for $Re = 100$ and in Fig. 9 for $Re = 250$. In each figure, there are two graphs, each for a different Rayleigh number. In interpreting these graphs, it is well to recall that $\theta = 1$ at the walls of the enclosure and $\theta = 0$ in the entering flow.

In Fig. 7, it is seen that the temperature fields for Rayleigh numbers between -10^6 and 10^4 are of the same character. Significant temperature variations are confined to the throughflow stream, while the steepest gradients occur adjacent to the upper wall, signaling relatively high rates of heat transfer. The remainder of the enclosure is nearly isothermal with slightly greater uniformity for $Ra = -10^6$ than for $Ra = 10^4$. The temperature rise (or drop) sustained by the throughflow stream during its passage through the enclosure is clearly in evidence in Fig. 7.

When the buoyancy forces first begin to draw the

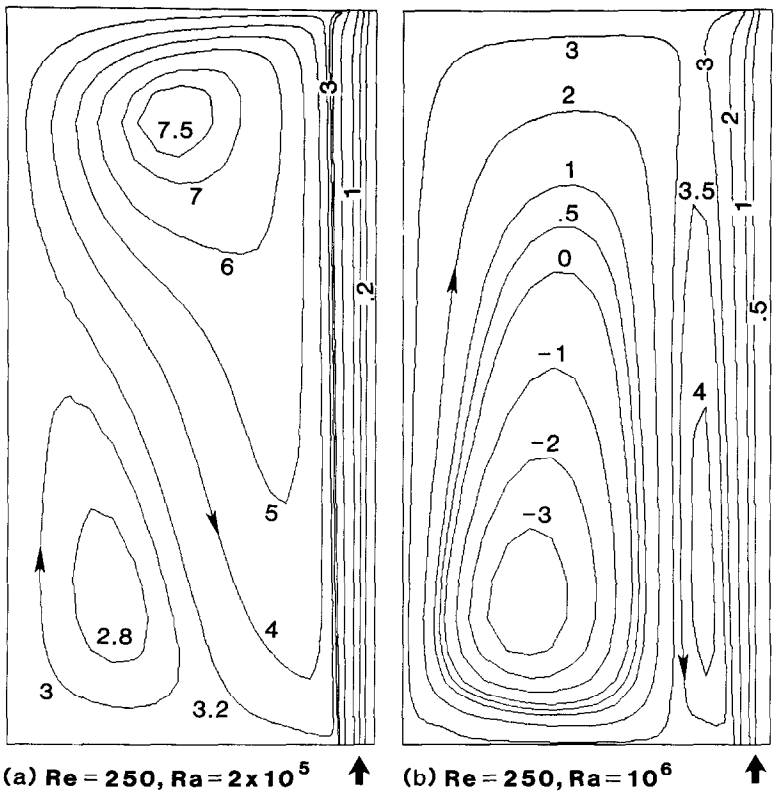

FIG. 6. Streamline maps for $Re = 250$, with $Ra = 2 \times 10^5$ and 10^6. The curve parameter is $\psi/\nu D$.

throughflow stream into the enclosure proper, the radial temperature variations, formerly confined to the core of the enclosure, penetrate out farther (Fig. 8, left-hand graph). Also a zone of steep axial gradients begins to develop adjacent to the lower wall owing to the passage of the throughflow stream in that neighborhood. When the buoyancy has annihilated the throughflow stream (right-hand graph), thermal stratification occurs in the upper portion of the enclosure. Steep temperature gradients exist near the lower wall and moderate temperature variations occur in the remnant of the throughflow stream. The region of highest wall heat flux is, clearly, adjacent to the lower wall.

The two isotherm maps in Fig. 9 for $Re = 250$ correspond to $Ra = -10^6$ and 10^6. The former reflects the full dominance of the throughflow-driven recirculation, with significant temperature variations confined to the throughflow stream and steep gradients in evidence adjacent to the upper wall. On the other hand, the latter corresponds to a buoyancy-driven recirculation zone occupying the enclosure, and the direction of this recirculation is just opposite to that of the aforementioned eddy that was driven by the throughflow. Thus, the bulges and steep gradients which are in evidence near the upper wall in the left-hand diagram of Fig. 9 occur near the lower wall in the right-hand diagram.

Surface-integrated heat transfer results

A listing of the surface-integrated heat transfer rates for the individual surfaces of the enclosure and for the enclosure as a whole is presented in Tables 1 and 2 respectively for $Re = 100$ and 250. In each table, there are successive columns for the lower, side, and upper surfaces and for the total heat transfer rate. The last column of the table is a ratio which shows the effect of the Rayleigh number on the total heat transfer rate. The numerator Q_t is the total heat transfer rate for $Ra \neq 0$, while the denominator Q_{t0} corresponds to $Ra = 0$ (pure forced convection). Values of $Q_t/Q_{t0} > 1$ signal heat transfer enhancement due to natural convection effects while $Q_t/Q_{t0} < 1$ indicates a natural-convection related reduction. The upper part of each table conveys information for $Ra \geq 0$, while the lower part is for $Ra \leq 0$.

Attention will first be turned to Table 1 and, specifically, to the results for positive Rayleigh numbers. From the table, it is seen that both the lower- and upper-surface heat transfer rates show regular trends with increasing Rayleigh number while the side wall displays a somewhat irregular pattern. These behaviors are readily understood with the aid of the flow and temperature field results which were presented earlier.

At low and intermediate Rayleigh numbers, where

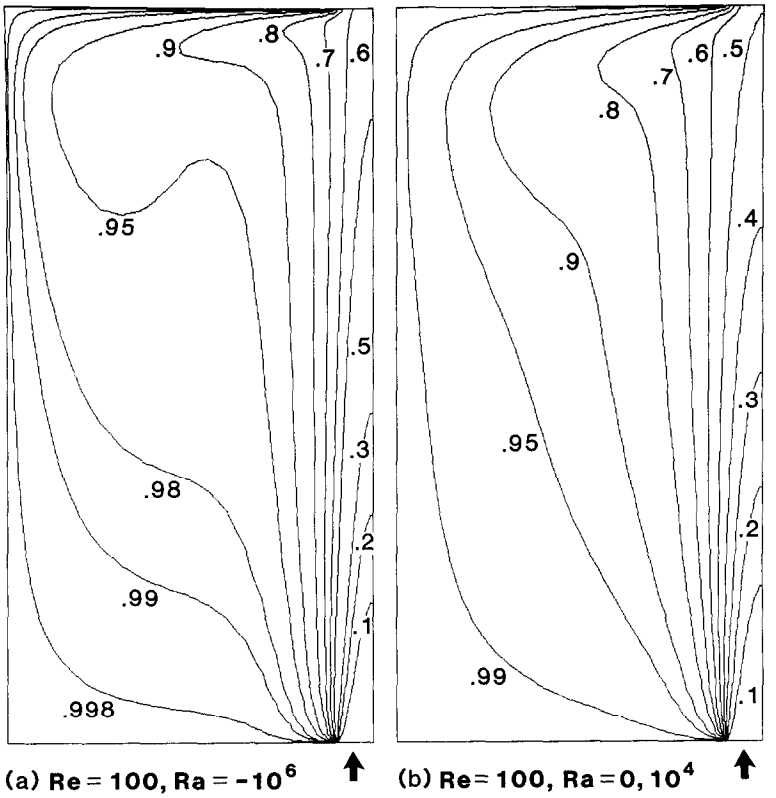

FIG. 7. Isotherm maps for $Re = 100$, with $Ra = -10^6$ and 0–10^4. The curve parameter is $\theta = (T - T_0)/(T_w - T_0)$.

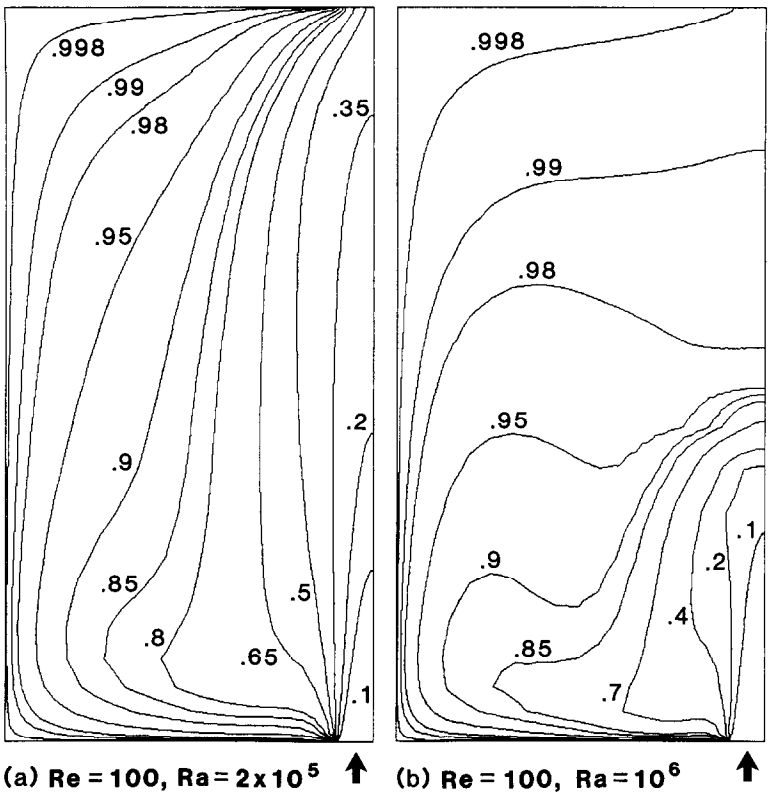

FIG. 8. Isotherm maps for $Re = 100$, with $Ra = 2 \times 10^5$ and 10^6. The curve parameter is $\theta = (T - T_0)/(T_w - T_0)$.

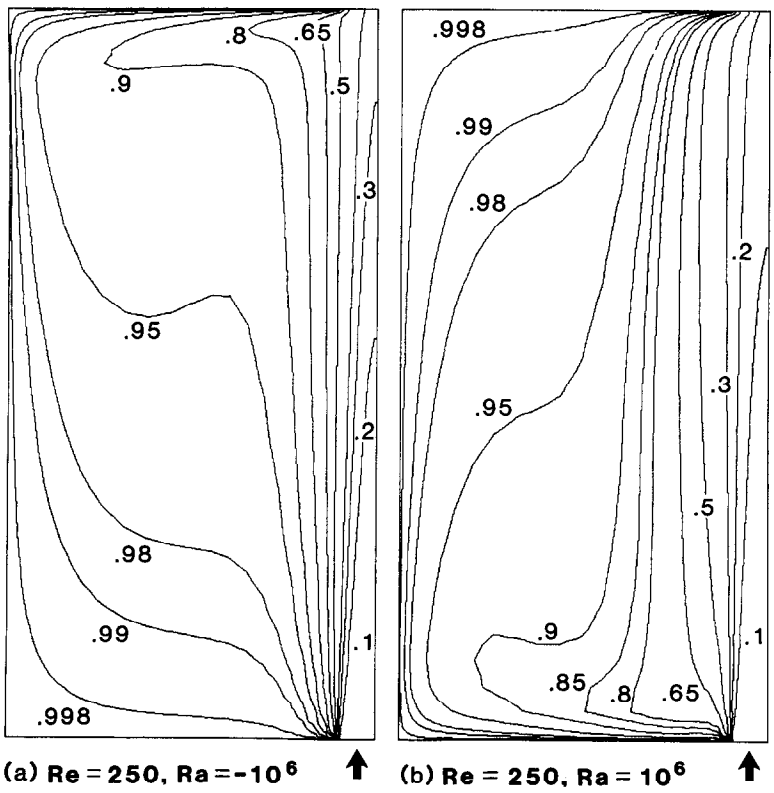

FIG. 9. Isotherm maps for $Re = 250$, with $Ra = -10^6$ and 10^6. The curve parameter is $\theta = (T - T_0)/(T_w - T_0)$.

Table 1. Surface-integrated heat transfer results, $Q/kD(T_w - T_0)$

	$Re = 100$				
Ra	Lower	Side	Upper	Total	Q_i/Q_{i0}
0	0.178	0.449	1.078	1.705	
10^3	0.178	0.449	1.078	1.705	1.000
10^4	0.183	0.446	1.071	1.700	0.997
10^5	0.449	0.452	0.688	1.589	0.932
2×10^5	1.030	0.770	0.163	1.963	1.151
5×10^5	1.671	1.034	0.0232	2.728	1.600
10^6	1.888	0.839	0.117	2.739	1.606
0	0.178	0.449	1.078	1.705	
-10^3	0.178	0.449	1.078	1.705	1.000
-10^4	0.174	0.452	1.084	1.710	1.003
-10^5	0.155	0.462	1.112	1.729	1.014
-10^6	0.116	0.456	1.162	1.734	1.017

the enclosure is filled with a recirculation zone that is driven by the throughflow stream, the highest rates of heat transfer occur on the upper surface, with lesser transfers at the other surfaces. This distribution is consistent with the direction of the recirculation, whereby the recirculating fluid successively washes the upper, side, and lower walls. The buoyancy-induced opposition to this flow pattern is reflected in a modest decrease in the upper- and side-wall heat transfer and an increase in the lower-wall heat transfer (see table entry for $Ra = 10^4$). When the buoyancy is strong enough to create an oppositely directed recirculation zone in the outer portion of the enclosure ($Ra = 10^5$), the respective increases and decreases at the lower and upper walls become more marked.

The deflection of the throughflow stream along the lower and side walls which occurs at higher Rayleigh numbers ($Ra = 2 \times 10^5$ and 5×10^5) results in major heat transfer increases at both these walls, at the expense of a sharp decrease at the upper wall. These trends continue at $Ra = 10^6$, but there is a reduction at the side wall which is believed to result from the incipient thermal saturation of the flow, which experiences high rates of heat transfer at the lower wall before it encounters the side wall. Furthermore, at the high Rayleigh numbers, the upper wall has essentially ceased to transfer heat.

With regard to the total heat transfer, it is seen to suffer a reduction when the buoyancy plays an opposition role to a dominant throughflow-driven eddy. Once the natural convection has won control of the flow field in the enclosure, there is a marked increase in the heat transfer, which tends to level off at the highest Rayleigh number investigated.

The lower portion of Table 1, which pertains to $Ra \leq 0$, will now be examined. Negative-Rayleigh-number buoyancy tends to reinforce the throughflow-driven recirculation, but with only modest effects on the flow field in the investigated range of Ra (Fig. 2). Correspondingly, the ranking of the upper wall as the primary heat transfer surface is maintained and even moderately enhanced. With increasing magnitude of $-Ra$, the lower wall progressively transfers less heat while the upper wall transfers more heat; the side wall experiences an indecisive fluctuation. The net effect on the total heat transfer is a variation of less than 2% over the investigated range of $Ra \leq 0$.

Attention will next be turned to the results for $Re = 250$ which are displayed in Table 2, with first consideration given to $Ra \geq 0$. For this higher Reynolds number, there is a greater range of Rayleigh numbers where the buoyancy plays an opposition role with respect to a dominant throughflow-driven recirculation. This is reflected, for example, by the total heat transfer, which declines as Ra increases from 0 to 5×10^5 and then recovers at $Ra = 10^6$ as the buoyancy establishes a strong eddy in the outer portion of the enclosure. At still higher Rayleigh numbers, buoyancy builds up and Q_i/Q_{i0} ratios above unity are to be expected. The side-wall heat transfer also declines with Ra until the buoyancy strongly asserts itself, with a subsequent increase. At the lower and upper walls, the respective trends of increase and decline, already evidenced in Table 1, continue in force, as they should.

The lower part of Table 2 reaffirms the main findings already encountered in Table 1 for $Re \leq 0$. There are some differences in detail, but the total heat transfer demonstrates the same insensitivity to Rayleigh number.

From an overview of Tables 1 and 2, it is evident that a first-impressions prediction of the enhancing or degrading effect of natural convection on the forced-convection heat transfer may be erroneous. Based on experience with simple vertical-plate boundary layer flows, it would be expected that the buoyancy associated with $T_w > T_0$ ($Ra > 0$) would enhance a forced-convection upflow. Such an enhancement does occur in the present enclosure problem at sufficiently high Rayleigh numbers, but only beyond a threshold Rayleigh number (which depends on the magnitude of the Reynolds number), below which the enclosure heat transfer is reduced by the buoyancy. Another somewhat surprising finding from the tables is the near independence of the enclosure heat transfer from the Rayleigh number when $T_w < T_0$.

Table 2. Surface-integrated heat transfer results $Q/kD(T_w - T_0)$

	$Re = 250$				
Ra	Lower	Side	Upper	Total	Q_i/Q_{i0}
0	0.113	0.635	2.020	2.768	
10^3	0.113	0.635	2.020	2.768	1.000
10^4	0.114	0.631	2.020	2.765	0.999
10^5	0.129	0.591	2.017	2.737	0.989
2×10^5	0.173	0.512	1.995	2.680	0.968
3×10^5	0.342	0.358	1.869	2.569	0.928
5×10^5	0.691	0.399	1.338	2.428	0.877
10^6	1.301	0.741	0.462	2.504	0.905
0	0.113	0.635	2.020	2.768	
-10^3	0.113	0.638	2.020	2.771	1.001
-10^4	0.112	0.638	2.020	2.770	1.001
-10^5	0.105	0.663	2.020	2.788	1.007
-10^6	0.0892	0.729	2.023	2.841	1.026

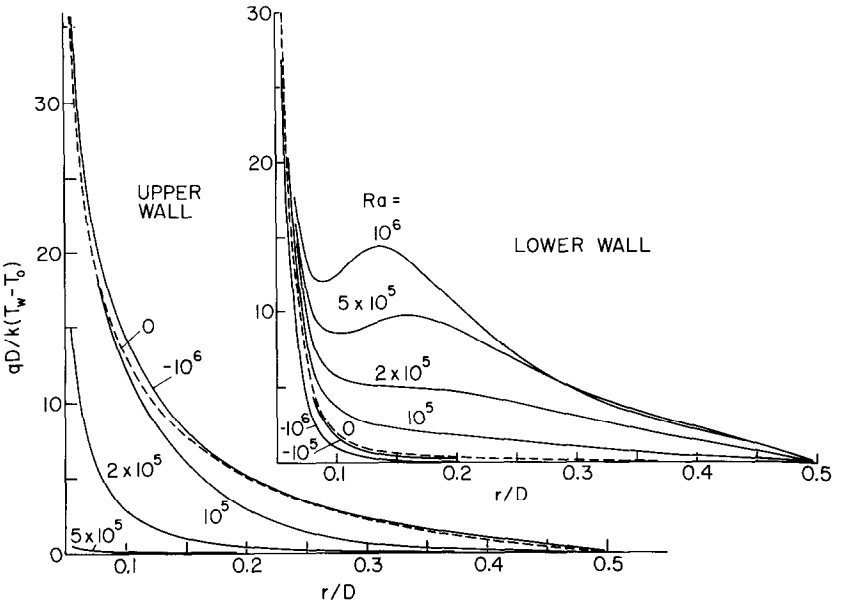

FIG. 10. Distributions of the local heat flux along the upper and lower walls of the enclosure, $Re = 100$.

Local heat transfer distributions

Distributions of the local rate of heat transfer per unit area along the upper and lower walls of the enclosure are presented in Fig. 10 for $Re = 100$, while Fig. 11 conveys the distributions for the side wall. A corresponding presentation for $Re = 250$ is made in Figs. 12 and 13. In these figures, a dimensionless heat flux group $qD/k(T_w - T_0)$ is plotted as a function of either r/D or z/D, with the coordinates being illustrated in the right-hand diagram of Fig. 1. The curves are parameterized by the Rayleigh number, which extends over both positive and negative values. Owing to crowding and overlap among the curves, it is not possible to include results for all the investigated Rayleigh numbers in Figs. 10–13, but those appearing in the figures are representative.

From Fig. 10, it is seen that the distribution curves for the lower wall are arranged in ascending order with increasing Rayleigh number while those for the upper wall are in descending order. These orderings are the same as those of the surface-integrated heat transfer that were identified in connection with Table 1, and the explanations that were set forth there are equally applicable here.

With regard to the spatial variations of the heat flux, Fig. 10 shows that the highest values at both the upper and lower walls are attained at the innermost radius, from which point the flux decreases as the radial coordinate increases. The radial decrease is monotonic at the upper wall for all Rayleigh numbers, despite the fact that the direction of the recirculation reverses over the investigated range of Rayleigh number. The monotonic behavior is related to the fact that the boundary layer thickness increases in the radially outward direction for both the clockwise and counterclockwise recirculation patterns. At the lower wall, the radial decrease of the flux is also monotonic for negative and for positive Rayleigh numbers up to 2×10^5. However, for higher Rayleigh numbers, there is a local maximum in the flux at an intermediate radial station. As can be seen from Fig. 4, this behavior is due to the reattachment of the deflected throughflow stream on the lower wall.

Figure 11 conveys the local heat flux distributions along the side wall. The striking characteristic of these distributions is the shift of the maximum heat flux from the upper portion of the wall to the lower portion of the wall as the Rayleigh number increases. This shift is directly related to the reversal of the direction of the recirculating motion which accompanies the transition from throughflow dominance to buoyancy dominance. The very low heat flux adjacent to the corners $z/D = 0$ and 1 is due to the very low velocities that prevail in those regions.

The local heat transfer results for the upper and lower walls for $Re = 250$, shown in Fig. 12, display characteristics similar to those already discussed for the case of $Re = 100$ in connection with Fig. 10. The main difference between the two sets of results is the lesser influence of natural convection. Thus, for example, the local maximum in the lower-wall heat flux distribution for $Ra = 10^6$ is much less pronounced when $Re = 250$ than when $Re = 100$. Also, the upper-wall heat flux distribution for $Ra = 10^6$ is clearly in view when $Re = 250$ but has dropped out of sight for $Re = 100$.

The side-wall heat transfer distributions for $Re = 250$ (Fig. 13) also resemble those for $Re = 100$ (Fig. 11). However, for the former, there is a higher concentration of curve peaks in the upper portion of the wall. This behavior is due to the dominance of the throughflow-driven recirculation over a larger range of

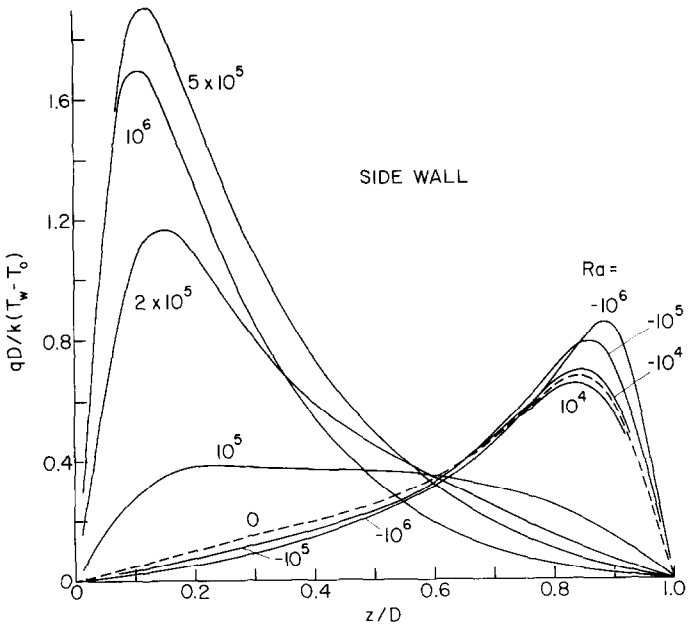

FIG. 11. Distributions of the local heat flux along the side wall of the enclosure, $Re = 100$.

Rayleigh numbers for $Re = 250$ than for $Re = 100$.

CONCLUDING REMARKS

The solutions presented here have set forth a succession of complex interactions between a throughflow stream passing through a vertical cylindrical enclosure and the buoyancy-induced motions within the enclosure which result from temperature differences between the entering stream and the enclosure walls. These interactions have a major influence on the heat transfer at the walls of the enclosure.

In the absence of buoyancy (i.e. zero Rayleigh number), the throughflow induces a large recirculating eddy in which the flow moves radially outward adjacent to the upper wall of the enclosure, downward along the side wall, and radially inward adjacent to the lower wall. Positive-Rayleigh-number natural convection ($T_w > T_0$) tends to induce a reversed direction for the recirculation. At small and intermediate Rayleigh numbers, the throughflow-driven recirculation is dominant, and the natural convection plays the role of a weaker opponent. As the Rayleigh number increases, a buoyancy-driven eddy is formed in the outer portion

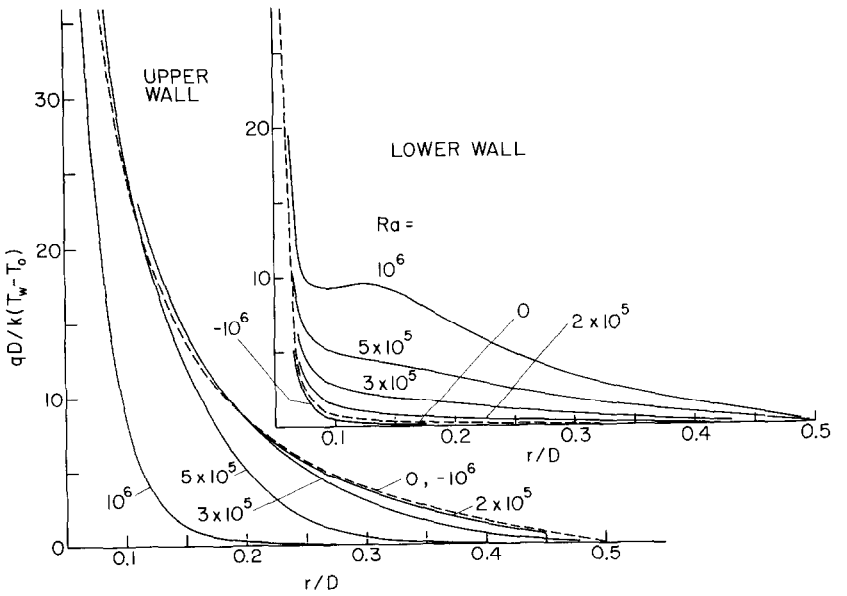

FIG. 12. Distributions of the local heat flux along the upper and lower walls of the enclosure, $Re = 250$.

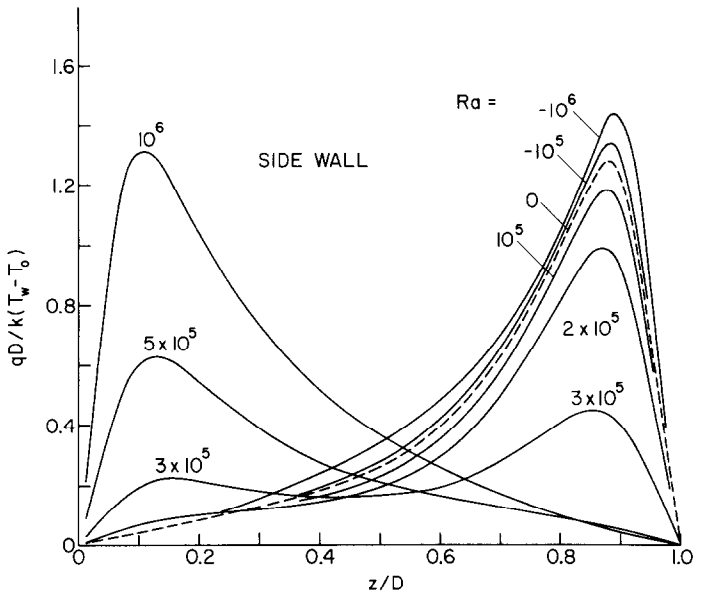

FIG. 13. Distributions of the local heat flux along the side wall of the enclosure, $Re = 250$.

of the enclosure, and this eddy grows and ultimately dominates the recirculating motion. At still higher Rayleigh numbers, the buoyancy draws the throughflow stream outward along the lower wall and propels it upward along the side wall—thereby signalling the full dominance of the natural convection. In contrast, negative-Rayleigh-number natural convection ($T_w < T_0$) reinforces the throughflow-driven recirculation, and the flow field in the enclosure is essentially unchanged from that without natural convection.

The temperature distributions within the enclosure show that the regions of large temperature gradients shift from the upper wall to the lower wall as the direction of the recirculation reverses owing to the transition from throughflow dominance to natural-convection dominance.

These events are reflected in both the local and surface-integrated heat transfer results. For positive Rayleigh numbers, the upper-wall heat transfer decreases as the Rayleigh number increases, with an opposite trend at the lower wall. At the side wall, there is an initial decrease in the heat transfer followed by an increase which, at sufficiently high Rayleigh numbers, may be followed by another decrease.

The surface-integrated heat transfer rate for the enclosure as a whole decreases as the Rayleigh number increases from zero, attains a minimum, and then increases. When the buoyancy is fully dominant (for positive Rayleigh numbers), the heat transfer is substantially larger than that for the buoyancy-free flow. For negative Rayleigh numbers, the heat transfer is very little different from that for zero Rayleigh number.

REFERENCE

1. S. V. Patankar, *Numerical Heat Transfer and Fluid Flow*. Hemisphere, Washington (1980).

INTERACTION DANS UNE ENCEINTE ENTRE UN ECOULEMENT FORCE ET LA CONVECTION NATURELLE

Résumé—On analyse l'écoulement et le transfert thermique dans une enceinte cylindrique verticale avec les parois inférieure et supérieure percées d'un petit trou par lequel le fluide entre et sort. Un écoulement de recirculation est induit par cette traversée en même temps que par la convection naturelle due à la différence de température entre le fluide et les parois de l'enceinte. Les paramètres caractéristiques sont les nombres de Reynolds et de Rayleigh, le dernier pouvant être positif ou négatif selon que la température de la paroi T_w dépasse ou non la température d'entrée du fluide T_0. Le courant forcé étant vertical ascendant, un nombre de Rayleigh positif ($T_w > T_0$) s'oppose à la recirculation due au courant forcé et il y a réduction du transfert thermique dans le domaine des nombres de Rayleigh faibles et moyens. Aux grands nombres de Rayleigh, l'écoulement est aidé par la convection naturelle et il en résulte de grandes valeurs de transfert thermique. Pour les nombres de Rayleigh négatifs ($T_w > T_0$), le transfert thermique est peu différent du cas où le nombre de Rayleigh est nul.

WECHSELWIRKUNG ZWISCHEN EINER STRÖMUNG, DIE DURCH EINEN HOHLRAUM FLIESST, UND FREIER KONVEKTION INNERHALB DES HOHLRAUMS

Zusammenfassung—Es wurde eine Untersuchung über die Fluidströmung und den Wärmetransport in einem vertikalen zylindrischen Hohlraum, in welchem das Fluid durch kleine Öffnungen am Boden und Deckel ein- bzw. ausströmt, durchgeführt. Die Durchgangs-Strömung erzeugt eine Rezirkulation in dem Raum. Weiterhin entstehen Bewegungen durch freie Konvektion infolge der Temperaturdifferenz zwischen einströmenden Fluid und den Hohlraumwänden. Die Stärke der erzwungenen und freien Konvektionsströmungen werden jeweils durch die entsprechenden Reynolds- und Rayleigh-Zahlen beschrieben, wobei letztere entweder positiv oder negativ sein können, je nachdem die Wandtemperatur T_w die Fluideintrittstemperatur T_0 übersteigt oder nicht. Ist die durchfließende Strömung vertikal nach oben gerichtet und ist eine positive Rayleigh-Zahl vorhanden (d.h. $T_w > T_0$), dann wirkt die freie Konvektion der durchflußbedingten Rezirkulation entegen und verringert den Wärmeübergang im Bereich kleiner und mittlerer Rayleigh-Zahlen. Für große Rayleigh-Zahlen überwiegt der Einfluß der freien Konvektion, und es ergeben sich hohe Wärmeübergangszahlen. Für negative Rayleigh-Zahlen (d.h. $T_w < T_0$) unterscheidet sich der Wärmeübergang nur wenig von dem Fall mit der Rayleigh-Zahl Null.

ВЗАИМОДЕЙСТВИЕ МЕЖДУ ПОТОКОМ, ПРОХОДЯЩИМ ЧЕРЕЗ ПОЛОСТЬ, И ЕСТЕСТВЕННОЙ КОНВЕКЦИЕЙ ВНУТРИ НЕЕ

Аннотация—Проведен анализ течения жидкости и теплопереноса в вертикально расположенной цилиндрической полости, в нижней и верхней стенках которой имеются небольшие отверстия, через которые втекает и вытекает жидкость. Сквозное течение вызывает рециркуляцию жидкости в полости. Кроме того, в ней возникают естественноконвективные течения из-за разности температур между поступающим потоком и стенками. Интенсивность вынужденной и естественной конвекции характеризуется соответственно числами Рейнольдса и Релея, причем последнее может быть положительным или отрицательным в зависимости от того выше или ниже температура стенки T_w температуры жидкости на входе T_0. В случае, когда струя направлена вертикально вверх, естественная конвекция при положительном числе Релея (т.е. при $T_w > T_0$) уменьшает вызываемую потоком рециркуляцию и снижает теплоперенос в диапазоне небольших и средних значений числа Релея. При больших числах Релея струйное течение усиливается за счет естественной конвекции, в результате чего увеличивается теплоперенос. При отрицательных значениях числа Релея (т.е. при $T_w < T_0$) теплоперенос почти такой же, как и при нулевом числе Релея.